Solitons and Their Biperiodic Pulsation in Ultrafast Fiber Lasers Based on CB/GO

Zhen-Tao Ju(居震涛), Zhi-Zeng Si(司志增), Xin Yan(严鑫), and Chao-Qing Dai(戴朝卿)*

College of Optical, Mechanical and Electrical Engineering, Zhejiang A&F University, Lin'an 311300, China

(Received 4 June 2024; accepted manuscript online 16 July 2024)

The carbon black (CB) is introduced to manufacture CB/graphene oxide (GO) composite material to mitigate limitations of GO as a saturable absorber with the excellent performance in ultrafast fiber lasers. At a central wavelength of 1555.5 nm, the stable mode-locked pulse with width of 656 fs, repetition rate of 20.16 MHz, and high signal-to-noise ratio of 82.07 dB is experimentally obtained. Additionally, experimental observations for pulsation phenomena of vector biperiodic solitons combining period-1 and period-17, period-2 and period-32, period-3 and period-36 are verified via simulations.

DOI: 10.1088/0256-307X/41/8/084203

Fiber lasers, as critical optical devices, play essential roles in fields such as communication, medical treatment, and material processing.[1–3] Their efficient, stable and high-quality laser outputs are highly favored. Unlike traditional lasers, fiber lasers have diverse cavity designs, including figure-eight cavities,[4] figure-nine cavities,[5] and ring cavities,[6] which significantly influence their performance parameters such as the mode selection, loss optimization, and output power. To achieve stable single-mode output and to optimize laser performance, various mode-locking mechanisms have garnered attention. Among these mechanisms, mode-locking technology with saturable absorber (SA)[7–9] is widely used to control and stabilize the output of fiber lasers. This technology[10,11] is based on the changes of nonlinear optical properties of SAs under high optical intensity, and enables stable control of laser output by adjusting the optical intensity.

In recent years, there are many high-performance materials suitably taken as SAs, such as HfS_3[12] and Bi_2Se_3.[13] Graphene oxide (GO), as a two-dimensional material, has gained significant attention in optics due to its excellent optical properties. However, traditional saturable absorber of GO has limitations, such as absorption loss, thermal effects and low optical damage thresholds. To overcome these issues, we introduce carbon black (CB),[14] a nanoscale carbon material, as an SA. CB is widely used in various fields, including plastics industry as an additive to improve mechanical strength and durability of plastics. CB possesses abundant porous structures, high surface area,[15] good light absorption, and SA characteristics. Additionally, CB is low-cost and easy to prepare, which makes it an ideal candidate for SA. By combining CB and GO, we can fully leverage the advantages of both materials, such as the durability of CB and the rapid response of GO, thereby to optimize the overall performance of the SA. The composite structure can extend the application range of the materials, and enhance their suitability for use in optics, electronics and energy fields, such as in ultrafast laser devices and optical modulators.

However, to date, there have been no reports on the performance of CB/GO composite as SA in fiber lasers. In this work, we successfully prepare the CB/GO composite and achieve the output of multiple types of soliton states using this composite material. We conduct a detailed investigation of the application of this composite material in fiber lasers and comprehensively evaluate its performance. This is significant for optimizing performance of fiber laser, as it promises higher-quality laser output and opens new possibilities for the further development of fiber laser technology.

Materials Preparation. In this experiment, the CB/GO film was prepared using a solution mixing method. The preparation process is as follows. Firstly, 0.105 g of CB powder was placed into an agate mortar and ground for 30 min. The ground CB powder was then transferred into 50 ml of deionized water and sonicated for 30 min, followed by stirring for another 30 min to fully integrate, the CB solution was derived. Next, 2 ml of the CB solution, 2 ml of GO solution, 2 ml of deionized water, and 0.09 g of polyvinyl alcohol (PVA) powder were added into a beaker and placed on a magnetic stirrer. The mixture was stirred continuously at a temperature of 27 ℃ and a speed of 500 r/min for one hour. Finally, 6 ml of mixed solution is poured into a polytetrafluoroethylene petri dish and dried in a drying oven at 60 ℃ for six hours to form the desired CB/GO composite SA film.

Experimental Setup. We constructed a 10.02-meter ring cavity, as illustrated in Fig. 1(a). The laser cavity comprises a pump source (LD), a wavelength division multiplexer (WDM), 0.4 meters of erbium-doped fiber (EDF), a polarization-independent isolator (PI-ISO), a polarization controller (PC1), a CB/GO-SA, a 5 : 5 optical coupler (OC), a polarization controller (PC2), and a polarization beam splitter (PBS). The output results were measured

*Corresponding author. Email: dcq424@126.com
© 2024 Chinese Physical Society and IOP Publishing Ltd

using an oscilloscope (DS2302B), an optical spectrum analyzer (Yokogawa AQ6370B), a radio-frequency (RF) spectrum analyzer (Keysight N9020A), and a commercial autocorrelator (APE Pulsecheck). The CB/GO film had a thickness of 13 μm in Fig. 1(b). Scanning electron microscope (SEM) images at 2 μm and 1 μm magnifications in Figs. 1(c) and 1(d) reveal slight surface wrinkles and a layered structure, respectively. The Raman spectrum in Fig. 1(e) indicates typical CB/GO characteristics: the strong peak in 1305 cm^{-1} signifies disordered carbon structures or defects in GO, while the peak in 1575 cm^{-1} indicates symmetric stretching vibrations of sp^2-hybridized carbon atoms in CB and graphene. These peaks affirm the feasibility of CB/GO composite as an SA.

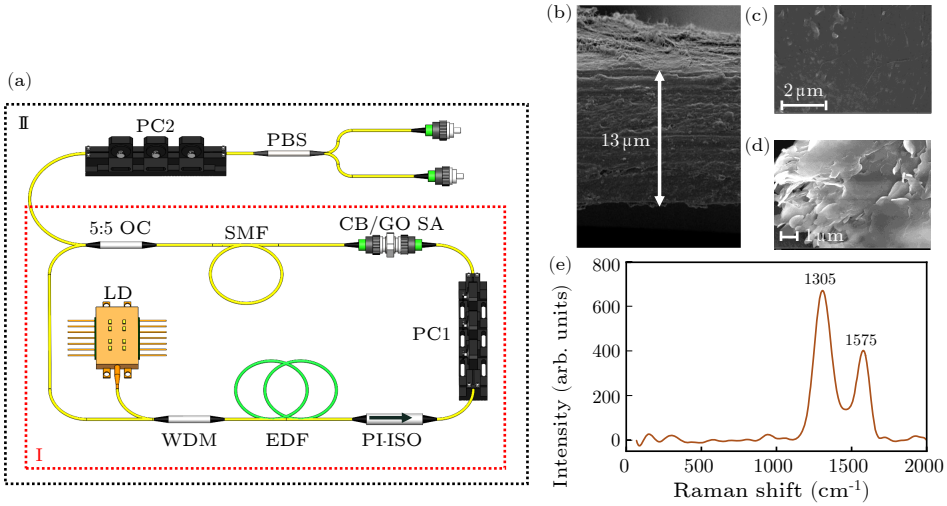

Fig. 1. (a) Cavity scheme of the fiber laser for generation of (I) conventional soliton and (Ⅱ) pulsating soliton, (b) thickness of the CB/GO film, [(c), (d)] different magnifications of SEM images for CB/GO, and (e) Raman spectrum of CB/GO.

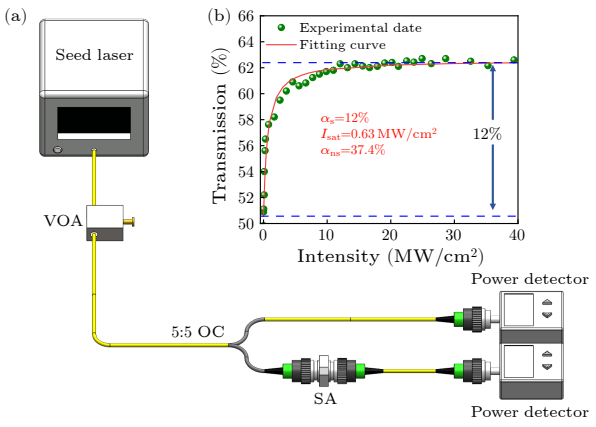

Fig. 2. (a) Setup of a dual-balanced detection measurement and (b) nonlinear SA curve.

This experiment employed a dual-balanced detection system as depicted in Fig. 2(a), to assess the nonlinear absorption properties of CB/GO material. The measured data are utilized to fit the SA curve of the CB/GO film, with the fitting function given by

$$\alpha(I) = \frac{\alpha_s}{1 + I/I_{sat}} + \alpha_{ns}, \tag{1}$$

where α_s represents the modulation depth, I_{sat} denotes the saturation intensity, and α_{ns} stands for the nonsaturable loss. The fitting results in Fig. 2(b) indicates that the modulation depth, saturation intensity, and nonsaturable loss are 12%, 0.63 MW/cm^2, and 34.7%, respectively.

Results and Discussion. In this experiment, we fabricated a CB/GO-SA film and achieve stable mode-locking within the ring cavity as illustrated in Fig. 1(a)-I. By toggling the pump on and off multiple times at 128 mW, stable self-starting mode-locking is achieved, and the output characteristics of the mode-locked pulse are shown in Fig. 3. Figure 3(a) shows the oscilloscope trace of the pulse sequence, with adjacent pulses spaced at 49.5 ns and a repetition rate of 20.16 MHz. Figure 3(b) displays the soliton spectrum during mode-locking as centered at 1555.5 nm with a 3 dB spectral width of 4.2 nm. The signal-to-noise ratio (SNR) is 82.07 dB at a repetition rate of 20.16 MHz in Fig. 3(c). The autocorrelation curve of the mode-locked pulse in Fig. 3(d) reveals a pulse width of 656 fs when it is fitted with a $sech^2$ curve. The time-bandwidth product (TBP) can be calculated using the following formula:

$$\mathrm{TBP} = c \cdot \frac{\Delta t \cdot \Delta\lambda}{\lambda^2}, \tag{2}$$

where c denotes the speed of light in vacuum, Δt represents the pulse width, $\Delta\lambda$ denotes the spectral width at 3 dB, and λ is the central wavelength of the spectrum. Calculations yield a TBP of 0.341, which indicates the slight chirp in the mode-locked pulses at this state.

To further validate the stability of the pulses, we adjusted the PC1 to obtain a stable spectral shape and recorded it per hour. After five hours of recording, the central wavelength of the spectrum was found to be stable at 1555.5 nm, as depicted in Fig. 3(e). In Fig. 3(f), it is evident that the output energy of the resonator increases linearly with the pump power, and exhibits a slope efficiency of 5.1% calculated for the mode-locked pulse. However, when the pump power reaches 195 mW, the mode-locking

ceases to be stable, and soliton splitting phenomena occur. The further increase of the pump power to 230 mW results in disappearance of the mode-locking.

To investigate the dynamic evolution and compression process of the intracavity pulse in the mode-locked laser based on CB/GO-SA, we conduct numerical simulations using the split-step Fourier method. The simulations employ the coupled nonlinear Schrödinger equation (CNLSE) to describe the system.

The coupled nonlinear Schrödinger equation (CNLSE) in the simulation reads

$$\begin{aligned}\frac{\partial u}{\partial z} &= \frac{i\Delta\beta}{2}u - \delta\frac{\partial u}{\partial t} - \frac{i\beta_2}{2}\frac{\partial^2 u}{\partial t^2} + \frac{g}{2}u + \frac{g}{2\Omega_g^2}\frac{\partial^2 u}{\partial t^2} \\ &\quad + i\gamma\left(|u|^2 + \frac{2}{3}|v|^2\right)u + \frac{i\gamma}{3}u^* v^2, \\ \frac{\partial v}{\partial z} &= \frac{i\Delta\beta}{2}u + \delta\frac{\partial v}{\partial t} - \frac{i\beta_2}{2}\frac{\partial^2 v}{\partial t^2} + \frac{g}{2}v + \frac{g}{2\Omega_g^2}\frac{\partial^2 v}{\partial t^2} \\ &\quad + i\gamma\left(|v|^2 + \frac{2}{3}|u|^2\right)v + \frac{i\gamma}{3}v^* u^2, \end{aligned} \tag{3}$$

where u and v are the amplitude envelopes of the two polarization components of vector solitons, $\Delta\beta = 2\pi/L_b$ is the wave vector difference, $\delta = \Delta\beta\lambda/2\pi c$ is the inverse group velocity difference with the beat length L_b; β_2, γ, and Ω_g are coefficients of group velocity dispersion (GVD), nonlinearity and gain bandwidth, respectively. The gain coefficient is expressed as

$$g = \frac{g_0}{1 + \int(|u|^2 + |v|^2)dt/E_{sat}}, \tag{4}$$

where g_0 is the small-signal gain and E_{sat} is the gain saturation energy. The Jones matrix is used to model the effect of the polarization controller (PC):

$$\begin{aligned} J_{PC} = &\begin{bmatrix}\cos(\theta) & -\sin(\theta) \\ \sin(\theta) & \cos(\theta)\end{bmatrix}\begin{bmatrix} e^{i\varphi/2} & 0 \\ 0 & e^{-i\varphi/2}\end{bmatrix} \\ &\cdot\begin{bmatrix}\cos(\theta) & \sin(\theta) \\ -\sin(\theta) & \cos(\theta)\end{bmatrix}, \end{aligned} \tag{5}$$

where θ is the rotation angle of the PC, and φ is the phase delay.

In the numerical simulation, the initial input pulse is a weak Gaussian pulse, and the fiber parameters used in the experiment are as follows: $L_{SMF} = 9.62$ m, $\beta_2 = -0.0198\,\text{ps}^2/\text{m}$, $\gamma_{SMF} = 2\times10^{-3}\,\text{W}^{-1}$, $L_{EDF} = 0.4$ m, $\beta_2 = 0.013\,\text{ps}^2/\text{m}$, $\gamma_{EDF} = 3.6\times10^{-3}\,\text{W}^{-1}$, $\Omega_g = 30$ nm, $g_0 = 8\,\text{m}^{-1}$, $E_{sat} = 11.3$ pJ. The spectral width of the conventional soliton for the coupled parameters of u and v is 4.3 nm, and the pulse width is 660 fs, which are in good agreement with the experimental result.

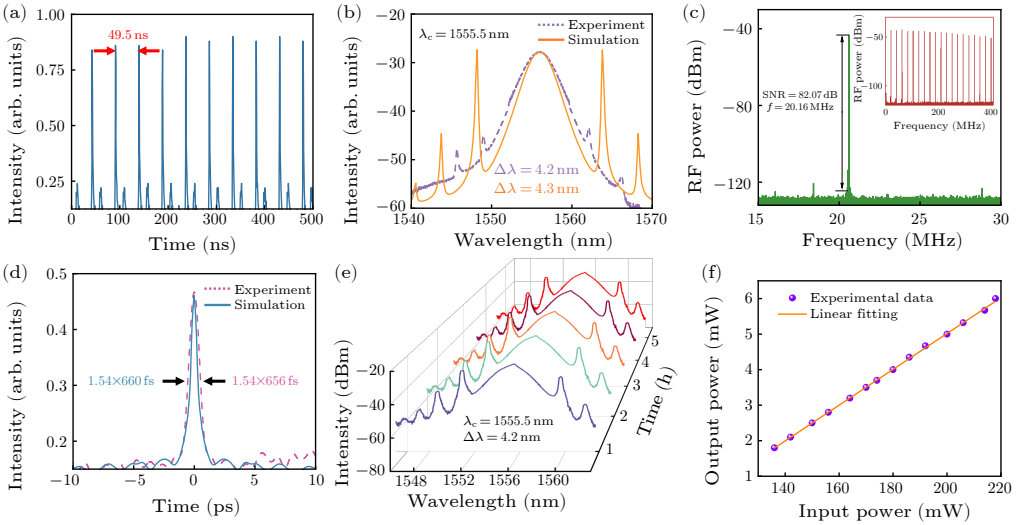

Fig. 3. Output performance of mode-locked pulse. (a) Oscilloscope trace, (b) optical spectrum, (c) RF spectrum and the broadband RF spectrum (inset), (d) autocorrelation trace, (e) five-hour continuous spectral output and (f) trend curve of output power.

Subsequently, we finely adjust the PC1 shown in Fig. 1(a)-Ⅱ and observe vector soliton pulsations on both components through PBS. In Fig. 4(a), the pulse intensities of the vertical and horizontal components of the vector biperiodic solitons are complementary.

From the experiment and simulation shown in Figs. 4(b) and 4(c), the consistency of the long and short periods corresponding to the vertical and horizontal components is confirmed. We specifically discuss the vertical component. By adjusting the PC1, vector biperiodic solitons composed of two pulsation periods $m + n$ (i.e., the combination of period-m and period-n) can be obtained. In Fig. 4(b)-(1), the short period is 1, and the frequency interval Δf_1 between the main and side peaks is 1.16 MHz, and the relationship of $f/\Delta f_1 \approx 17$ corresponds to the modulation period of 17 round trips (RTs) displayed on the pulse train, hence it is termed as $1 + 17$ (i.e., the combination of period-1 and period-17) biperiodic soliton. In Fig. 4(b)-(2), the frequency interval Δf_2 between the initial pulse and the vertical component is 9.8 MHz, and the relationship of $f/\Delta f_2 \approx 2$ indicates that the pulsating period is 2 RTs, and the frequency interval Δf_1 between the main and side peaks of the vertical component is 0.635 MHz, the relationship of $f/\Delta f_1 \approx 32$ corresponds

to the modulation period of 32 RTs displayed on the pulse train, hence it is termed as $2 + 32$ (i.e., the combination of period-2 and period-32) biperiodic soliton. Similarly, Fig. 4(b)-(3) is termed as $3 + 36$ (i.e., the combination of period-3 and period-36) biperiodic soliton.

To validate the realization of vector biperiodic solitons and obtain the key parameters affecting them, we use Eqs. (3), (4) and (5) to simulate the propagation of vector solitons in two polarization directions. Specific parameters in the simulation are same as those in Fig. 2 except for $g_0 = 12\,\mathrm{m}^{-1}$, $E_{\mathrm{sat}} = 6\,\mathrm{pJ}$. In the simulation, various types of vector biperiodic solitons are obtained in Fig. 4(b), when setting the rotation angle θ and the phase delay φ of the PC1 as $\theta = 0.04\pi$, 0.05π, 0.01π and $\varphi = 0.01\pi$, 0.018π, 0.066π, respectively.

From Fig. 4(b), the pulsation periods from the experiment and simulation are in good agreement. By adjusting the angles of the three blades (1), (2) and (3) of PC1 at different power levels, various-period pulsating solitons are obtained in Fig. 4(d), where counterclockwise (CCW) and clockwise (CW) directions are denoted as negative and positive values, respectively, and different colors denote different power levels, while varying sizes of spheres represent solitons with different periods, ranging from periods 1–4 + period-n pulsation period. From Fig. 4(d), at lower pump powers, solitons with 1–2 times pulsation period are more prevalent, while multiple-period pulsating solitons only emerge at higher pump powers. Overall, as the pump power approaches 195 mW, the variety of pulsation periods increases. This result can be applied to encoding,[16] considering its advantages of high stability, strong anti-interference capability, low power consumption and high data transmission rate to thereby enhance the reliability and efficiency of communication systems.

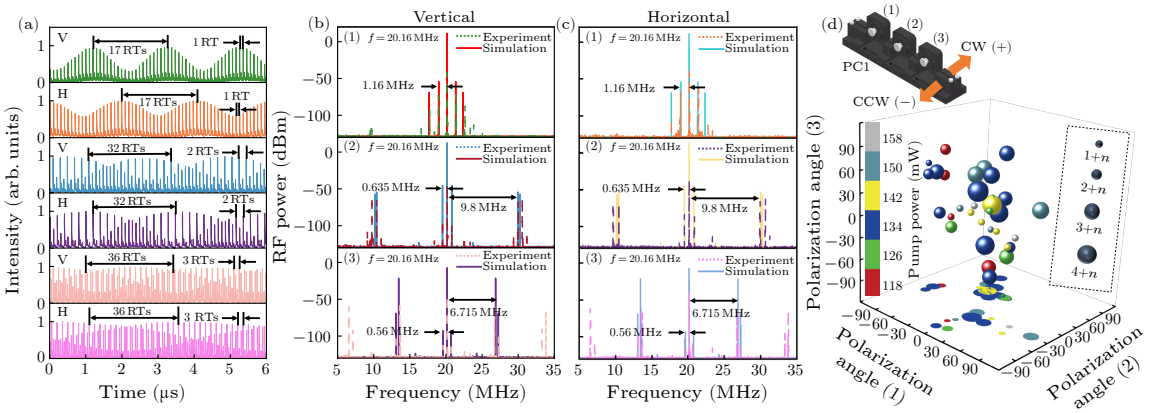

Fig. 4. Soliton pulsation with different periods. (a) Oscilloscope trace, [(b), (c)] broadband RF spectrum, and (d) different pulsation periods by changing the pump power and polarization angle of PC1. RT: round trips.

Table 1. Comparison of output results based on different two-dimensional material SAs.

Materials	Wavelength (nm)	Modulation depth	Pulse width (fs)	SNR (dB)	References
GO	1560	18.4%	1000	50.7	Ref. [17]
ZnO/GO	1563	18.69%	900	–	Ref. [18]
GO/PDMS	1557.05	4%	630	48.71	Ref. [19]
VSe_2/GO	1557.5	14.3%	573	60.4	Ref. [20]
CB/GO	1555.5	12%	656	82.07	This work

To further demonstrate the unique advantage and application value of CB/GO materials, we compare the experimental results with other materials in Table 1. In comparison, the CB/GO-SA exhibits narrower pulse width and higher SNR, which presents significant advantages in the field of fiber lasers, including improved signal quality, enhanced measurement precision, better communication quality, increased laser stability, and support for advanced applications. The high SNR of fiber lasers enables them to play a crucial role in various fields such as research, industry and communication to provide reliable and high-quality laser outputs.

In summary, we propose a fiber laser based on CB/GO-SA, and first prepare CB/GO film and successfully achieve mode-locked pulse with width of 656 fs, repetition rate of 20.16 MHz, and SNR of 82.07 dB. We then test the stability of the mode-locking and find that the spectral shape maintains unchanged over a continuous period of five hours. Furthermore, we experimentally realize vector biperiodic pulsating solitons composed of $1 + 17$, $2 + 32$, and $3 + 36$ long and short periods and verify them by numerical simulation. Finally, by comparison, we find that the composite material effectively compensates for the low damage threshold and high saturation absorption threshold defects of the original materials, and thereby achieve better stability of the pulses and providing new ideas for future SA selection.

Acknowledgments. This work was supported by the National Natural Science Foundation of China (Grant Nos. 12261131495 and 12475008), and the Scientific Research and Developed Fund of Zhejiang A&F University (Grant No. 2021FR0009).

References

[1] Fang Y, Han H B, Bo W B, Liu W, Wang B H, Wang Y Y, and Dai C Q 2023 *Opt. Lett.* **48** 779

[2] Fan Y, Zhang P, Liu Y, He S, Ning Y, and Wu T 2024 *Opt. Laser Technol.* **169** 110017

[3] Knall J, Engholm M, Boilard T, Bernier M, Vigneron P B, Yu N, Dragic P D, Ballato J, and Digonnet M J F 2021 *Optica* **8** 830

[4] Yuan Q, Wang T, Ma W, Ji H, Xiong H, and Xu Y 2021 *Appl. Opt.* **60** 2190

[5] Li X, Li S, Li X, Wang Y, Cheng Z, Xiong Y, Cao X, Feng Y, and Zhou J 2024 *Opt. Express* **32** 11271

[6] Huang W, Ma C, Li C, Zhang Y, Hu L, Chen T, Tang Y, Ju J, and Zhang H 2020 *Nanophotonics* **9** 2577

[7] Xiao Y J, Xing X W, Cui W W, Chen Y Q, Zhou Q, and Liu W J 2023 *Chin. Phys. Lett.* **40** 054201

[8] Wang H Y, Xiao Y J, Liu Q, Xing X W, Yang H J, and Liu W J 2023 *Chin. Phys. Lett.* **40** 114204

[9] Meng X C, Li L, Sun N Z, Xue Z, Liu Q, Ye H, and Liu W J 2023 *Chin. Phys. Lett.* **40** 124202

[10] Si Z Z, Dai C Q, and Liu W 2024 *Chin. Phys. Lett.* **41** 020502

[11] Si Z Z, Wang Y Y, and Dai C Q 2024 *Sci. China Phys. Mech. Astron.* **67** 274211

[12] Xing X, Liu Y, Han J, Liu W, and Wei Z 2023 *ACS Photon.* **10** 2264

[13] Li L, Xue Z, Pang L, Xiao X, Yang H, Zhang J, Zhang Y, Zhao Q, and Liu W 2024 *Opt. Lett.* **49** 1293

[14] Yablokov M Y, Shchegolikhin A N, Lebedev O V, Goncharuk G P, and Ozerin A N 2021 *Russ. Chem. Bull.* **70** 1816

[15] Jiao S, Liu M, Li Y, Abrha H, Wang J, Dai Y, Li J, Kang N, Li Y, and Liu X 2022 *Carbon* **193** 339

[16] Han H, Wang R, Cao H, Wen X, Dai C, Liu W, and Wang Y 2023 *Opt. Laser Technol.* **158** 108894

[17] Tsai L Y, Li Z Y, Lin J H, Song Y F, and Zhang H 2021 *Opt. Laser Technol.* **140** 106932

[18] Hassan H, Ariannejad M M, Safaei R, Amiri I S, and Ahmad H 2017 *IOP Conf. Ser. Mater. Sci. Eng.* **210** 012046

[19] Ng E K, Lau K Y, Lee H K, Abu Bakar M H, Mustapha Kamil Y, Omar M F, and Mahdi M A 2020 *Opt. Mater.* **100** 109619

[20] Wang B, Han H, Yu L, Wang Y, and Dai C 2021 *Nanophotonics* **11** 129